Elastic Properties of the Cell Surface and Trafficking of Single AMPA Receptors in Living Hippocampal Neurons

Alexandre Yersin,* Harald Hirling,* Sandor Kasas,* Charles Roduit,* Karina Kulangara,* Giovanni Dietler,† Frank Lafont,* Stefan Catsicas,* and Pascal Steiner*

*Brain Mind Institute, Faculté des Sciences de la Vie, and †Institut de Physique de la Matière Complexe, Faculté des Sciences de Base, Ecole Polytechnique Fédérale de Lausanne, Lausanne, Switzerland

ABSTRACT Although various approaches are routinely used to study receptor trafficking, a technology that allows for visualizing trafficking of single receptors at the surface of living cells remains lacking. Here we used atomic force microscope to simultaneously probe the topography of living cells, record the elastic properties of their surface, and examine the distribution of transfected α-amino-3-hydroxy-5-methylisoxazole-4-proprionic acid (AMPA)-type glutamate receptors (AMPAR). On nonstimulated neurons, AMPARs were located in stiff nanodomains with high elasticity modulus relative to the remaining cell surface. Receptor stimulation with *N*-methyl-D-aspartate (NMDA) provoked a permanent disappearance of these stiff nanodomains followed by a decrease (53%) of the number of surface AMPARs. Blocking electrical activity before NMDA stimulation recruited the same number of AMPARs for internalization, preceded by the loss of the stiff nanodomains. However, in that case, the stiff nanodomains were recovered and AMPARs were reinserted into the membrane shortly after. Our results show that modulation of receptor distribution is accompanied by changes in the local elastic properties of cell membrane. We postulate, therefore, that the mechanical environment of a receptor might be critical to determine its specific distribution behavior in response to different stimuli.

INTRODUCTION

Trafficking of neuronal receptors is directly implicated in synaptic plasticity and is fundamental for proper neuronal communication (1,2). α-amino-3-hydroxy-5-methylisoxazole-4-proprionic acid (AMPA)-type receptor (AMPAR), located at excitatory synapses, is activated by the neurotransmitter glutamate. AMPARs mediate most of rapid excitatory neurotransmission in the mammalian central nervous system. Four different AMPAR subunits (GluR1-4) can assemble together as homo- or heterotetramers to form a receptor whose properties will depend on its composition (3,4). In the mammalian hippocampus, a brain region involved in memory encoding, the GluR1/2 and GluR2/3 assemblies are predominant. The number of AMPARs present at the synapse is highly regulated in an activity-dependent manner. It was recently shown that exocytic insertion and endocytic removal of AMPARs at the neuronal plasma membrane (4,5) as well as their lateral diffusion (6,7) are major determinants of synaptic strength. Depending on specific pharmacological stimuli, surface AMPARs are internalized and subsequently sorted to differential intracellular pathways (3,5,8). Recent studies have allowed significant advances in understanding the molecular determinants involved in regulating receptor trafficking processes (9–11). It has also been shown that cholesterol/sphingolipid microdomains are associated with AMPARs in dendrites (12).

Techniques routinely used to study receptor trafficking cannot reach the single molecule resolution and often do not allow real-time measurements. A technology that allows one to study the distribution of single receptors at the surface of living cells remains, therefore, lacking. To address theses issues, we took advantage of the versatility of atomic force microscopy (AFM). Besides its initial imaging functions (13,14), AFM is nowadays widely used to study single molecule interactions (15,16), molecular unfoldings (17,18), and mechanical properties of the cells (19). Measuring a ligand-receptor interaction at the level of single molecules is achieved by functionalizing an AFM tip with the ligand molecule and probing either a surface functionalized with the receptor molecule (20–22) or a cell presenting the receptor at its surface (23–25). As pointed out by Ikai (26), a ligand-receptor interaction measurement would be pointless on cells if the force required to uproot the receptor is lower than the force necessary to disrupt the interaction. However, receptor extraction forces generally appear to be stronger than protein-protein interaction forces (27,28) and various ligand-receptor interactions have been successfully measured at the cell surface (23–25). Furthermore, this type of experiment has allowed mapping the presence of specific receptors at the surface of living cells (29–31).

Submitted July 4, 2006, and accepted for publication February 21, 2007.

Address reprint requests to Alexandre Yersin, E-mail: ayersin@bio.titech.ac.jp; or Pascal Steiner, E-mail: pascal_steiner@hms.harvard.edu.

Alexandre Yersin's present address is Laboratory of Biodynamics, Graduate School of Bioscience and Biotechnology, Tokyo Institute of Technology, 4259-B8 Nagatsuta, Midori-ku, Yokohama, 226-8501, Japan.

Frank Lafont's present address is Institut Pasteur de Lille, 1 rue du Prof. Calmette, 59019, Lille, France.

Pascal Steiner's present address is Dept. of Neurobiology, Harvard Medical School, 220 Longwood Ave., Boston, MA 02115.

0006-3495/07/06/4482/08 $2.00

doi: 10.1529/biophysj.106.092742

Mechanical properties of living cells are measured by AFM using the tip as an indenter that slightly presses the cell. Forces transmitted to the cantilever during the tip indentation process are analyzed and provide access to local values of the elastic modulus (32,33). Such measurements have been applied to map the elastic properties of various cells and to record the mechanical changes that occur after drug application (31,34–36).

In this study, we used AFM to simultaneously detect AMPARs at the surface of living neurons and measure the biophysical properties of the cell surface at and around the receptor site. Moreover, we provide a dynamic sequence of events following pharmacological stimulations.

MATERIALS AND METHODS

Cell culture and transfection

Hippocampal neuron cultures were prepared from newborn rats as described (37). Neurons were transfected at P8 by the calcium phosphate method (38) with plasmids encoding for either both green fluorescent protein (GFP) and hemagglutinin (HA)-GluR2 (kindly provided by Dr. M. Passafaro, Milan, Italy) or for GFP alone when indicated. Briefly, 4 μg DNA per each 35-mm dish were mixed with 200 mM $CaCl_2$ in a final volume of 60 μl and added gently to the same volume of HEPES buffered saline (HBS) 2× pH 7.07–7.12 (274 mM NaCl, 10 mM KCl, 1.4 mM Na_2HPO_4, 15 mM D-Glucose, 42 mM HEPES, pH 7.4). The mix was then incubated at room temperature for 30–40 min and added dropwise to each plate. The incubation was stopped after 30 min by adding glycerol shock solution (HBS 1×, 10 mM $MgCl_2$ in 5 mM HEPES, pH 7.5, 5% glycerol) for 1 min. Cells were then rinsed with wash medium.

Between P14 and P17, medium was exchanged with K5 (128 mM NaCl, 5 mM KCl, 2.7 mM $CaCl_2$, 10 mM glucose, 20 mM HEPES, 1 mM $MgCl_2$, pH 7.4, heated at 37°C) and AFM experiments were performed. When specified, tetrodotoxin ((TTX), 2 μM) was added to the buffer to block spontaneous electric activity (5). When indicated, hypertonic conditions were produced by adding 450 mM sucrose in K5 solution to prevent clathrin-mediated endocytosis (39). Immunocytochemistry (Fig. 1, *A* and *B*) on 4% paraformaldehyde/4% sucrose fixed neurons was performed as described (40).

AFM tip preparation

Silicon nitride cantilevers (Veeco, Santa Barbara, CA; nominal spring constant 0.06 N/m) were calibrated according to thermal fluctuation analysis (41). To remove any possible organic residues, the tips were immersed 5–10 s in piranha solution (75% H_2SO_4, 25% H_2O_2) and extensively cleaned with phosphate buffered saline (PBS). HA antibodies were cross-linked to AFM tips using 1-ethyl-3 [3-(dimethylamino)propyl] carbodiimide (EDC) as a coupling agent (42). The tips were immersed in 100 μl MES (0.1 M, pH 6) containing 5–7 μg of antibody for 1 h, then 100 μl MES with 0.13 mg EDC were added for 2 h. The tips were then transferred in 100 μl glycine (0.1 M, pH 2.5) for 10 min to neutralize free EDC molecules, then extensively washed with PBS and stored at 4°C in PBS until use.

AFM measurements

We used a commercial AFM (Bioscope, Veeco) mounted on an inverted optical microscope (Axiomat, Zeiss, Jena, Germany) equipped with fluorescence light. This setup allowed us to locate transfected cells through GFP illumination and to position the tip above the cell body.

Tips prepared as described above were alternately approached and retracted from the cell body surface (Fig. 1 *C*). The cantilever deflections resulting from these approach/retraction cycles were monitored as a function of the *z* axis extension, providing approach and retraction force curves (see Fig. 2 *A*). An array of 16 × 16 force curves was recorded on the cell body surface, covering an area of 2 × 2 μm with pixels of 125 × 125 nm (force mapping, Fig. 1 *D*). The array was recorded line by line and the scan time required to obtain one array was ~2 min (cantilever approach/retraction speed 5.6 μm/s). The force applied on the cells was maintained below 1 nN, which caused a tip indentation of 100–200 nm. The contact area between the tip and the cell was, therefore, similar to the surface of one pixel of the array, as previously shown (30).

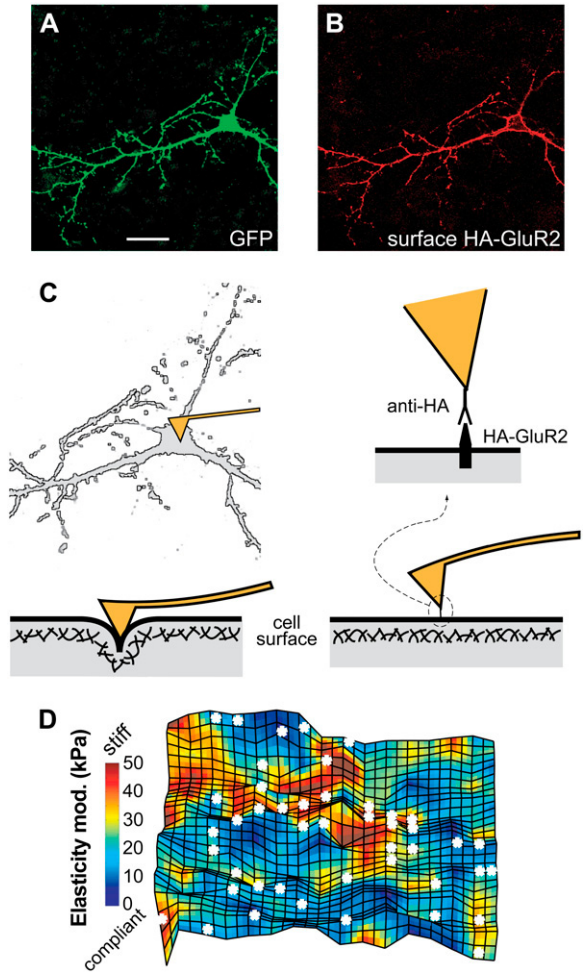

FIGURE 1 On-line detection of the HA-tagged AMPAR subunit GluR2 at the surface of living hippocampal neurons by AFM. (*A* and *B*) Confocal sections of a cultured hippocampal neuron overexpressing GFP and HA-GluR2 that was fixed and immunostained with a HA-antibody under nonpermeabilized conditions. Shown are the GFP signal (*A*) and anti-HA labeled surface GluR2 (*B*). Scale bar is 15 μm. (*C*) Experimental setup used to scan living neurons with an AFM tip functionalized with HA-antibodies. Indentation of the tip into the cell (*bottom left*) provides local elasticity measurements. Cantilever retraction (*bottom right*) is used to detect interactions between the anti-HA tip and surface HA-GluR2 (*top right*), which helps locating HA-tagged AMPAR at the cell surface. (*D*) Topographic map of a scanned cell surface (2 × 2 μm). Asterisks mark detected binding-unbinding event between HA-antibodies and HA-tagged GluR2. Color code represents local values of the elasticity modulus, which reflects the cell stiffness. The map was smoothened by linearly extrapolating intermediate values between the subdivisions.

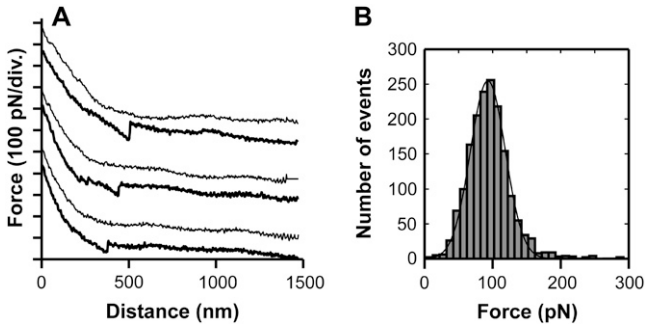

FIGURE 2 (*A*) Force curves displaying the AFM cantilever deflection as a function of its vertical *z*-position. Thick lines are retraction force curves displaying binding-unbinding events between the anti-HA tip and HA-tagged AMPARs. Thin lines are the corresponding approach curves (slightly shifted upward to increase visibility). (*B*) Force histogram of the unbinding events recorded between the anti-HA tip and HA-tagged AMPARs at the cell surface. The mean rupture force (±SD) is 92 ± 26 pN (Gaussian fit), performed at a mean loading rate of 10,000 nN/s.

N-methyl-D-aspartate (NMDA) stimulations were performed through a homemade injection system. When indicated, cells were stimulated for 2 min with 50 μM NMDA and then washed three times with K5 (or K5 with 2 μM TTX when specified).

Data analysis

Elasticity modulus E of the cell cortex was calculated according to an adaptation of the Hertz model describing the indentation of a stiff cone in a soft sample (32,43). This model predicts that a loading force F will produce an indentation δ according to the relation:

$$F = \delta^2 \frac{2}{\pi} \frac{E}{(1-\nu^2)} \tan\alpha,$$

where α is the half-opening angle of the AFM tip (35° here) and ν is the Poisson's ratio, assumed to be 0.5 for cells. Force-indentation curves were obtained from the approach force curves by using a reference curve recorded on the hard cell substrate as calibration (33). We restricted the analysis of indentation curves to a low range of loading force, varying between 0.1 and 0.5 nN (50 nm of indentation). E was obtained by adjusting a linear fit to a F vs. δ^2 plot. To determine the contact point between the tip and the cell surface, we estimated the standard deviation of cantilever deflections on the off-contact part of the approach curve. The contact point was taken as the point where the upward cantilever deflection exceeded twice this value.

Binding-unbinding events between the anti-HA tip and surface HA-tagged AMPARs were identified by a characteristic signal on the retraction force curves (Fig. 2 *A*). These events were analyzed off-line by a fuzzy logic algorithm developed in our laboratory (44) and were used to locate the position of HA-tagged AMPARs at the cell surface.

To compare the elasticity of receptor sites with their vicinity, the elastic modulus of each pixel containing a receptor was divided by the average elastic modulus of the pixels situated 250 nm away from the receptor on the same scan line (vicinity site). If a vicinity site was coinciding with a receptor site, it was not included in the calculation. Sites distant from receptors were chosen as the pixels situated farther than 250 nm away from any receptor. To test the effect of NMDA stimulation on the whole scanned surface, the average elasticity modulus of the global area before stimulation was compared with the value obtained after stimulation. All the elasticity measurements presented here are therefore relative values, which allows one to circumvent the problems that may arise from absolute measurements (45).

Statistical analysis

All n-values reported here are related to a number of cells. On Fig. 3 *C*, for all tested cells ($n = 12$), the mean percentage of curve presenting 1, 2, or 3 events were calculated and a paired two-tailed t-test was applied to these means. On Fig. 4 *A*, for all tested cells the mean number of events recorded on a 2 × 2 μm surface was calculated and a paired two-tailed t-test was applied between the three different populations. For Fig. 5 *A*, the mean values of relative elasticity at 125 nm, at 250 nm, and farther from the receptor were calculated for each cell ($n = 6$). We then applied a paired two-tailed t-test between those values. On Fig. 6, *A* and *B*, we applied an unpaired two-tailed t-test between all the values recorded for NMDA treated cells ($n = 5$) and all the control values ($n = 6$ cells) measured after the initial decrease observed on NMDA curves. On Fig. 6, *C* and *D*, at each time point an unpaired two-tailed t-test was applied between the values recorded for NMDA/TTX treated cells ($n = 6$) and the control values ($n = 6$ cells).

RESULTS

Mapping receptors, elasticity, and topography on living cells

To study the real-time distribution of single receptors with AFM, AMPARs tagged with an extracellular peptide (HA-tag) were expressed at the surface of living cells. We cotransfected hippocampal neurons with the HA-tagged AMPAR subunit GluR2 (HA-GluR2) and GFP for identification of transfected cells (Fig. 1 *A*). Transfected GluR2 subunits have been reported to form homomeric GluR2/2 AMPARs whose trafficking behavior is similar to that of the endogenous hetero-oligomeric GluR2/3 receptors (46). Confocal microscopy showed that transfected HA-GluR2/2 AMPARs were expressed at the surface of cell bodies and processes, with the HA-tag facing the extracellular medium (Fig. 1 *B*), as previously described (4). Therefore, an AFM tip functionalized with an anti-HA antibody (anti-HA tip) was used as a probe to detect surface HA-tagged AMPARs, as illustrated in Fig. 1 *C*. Anti-HA antibody molecules were covalently bound to AFM tips by a carbodiimide coupling reaction (see Materials and Methods).

GFP-positive neurons were identified and scanned with an anti-HA tip. Two-dimensional arrays of 16 × 16 force curves were recorded on a 2 × 2 μm square with subdivisions of 125 × 125 nm on the soma of GFP/HA-GluR2-cotransfected neurons (Fig. 1 *D*). Approach force curves (Fig. 2 *A*) provided access to the local elasticity modulus, which reflected the stiffness of the cell surface (Fig. 1 *D*, *false colors*). Binding-unbinding events between the anti-HA tip and surface HA-tagged AMPARs (Fig. 2 *A*) showed that the mean force necessary to unbind the molecules was 92 ± 26 pN (Fig. 2 *B*). Moreover, they enabled us to map the location of receptors on the cell surface (Figs. 1 *D* and 3 *A*, *white spots*). Therefore, this approach allowed us to correlate the spatial distribution of single AMPARs with the relative cell elasticity at any given time.

We examined whether topography and elasticity measurements, independently of receptor presence, would correlate on living cells. Neurons ($n = 24$ cells) displayed an irregular

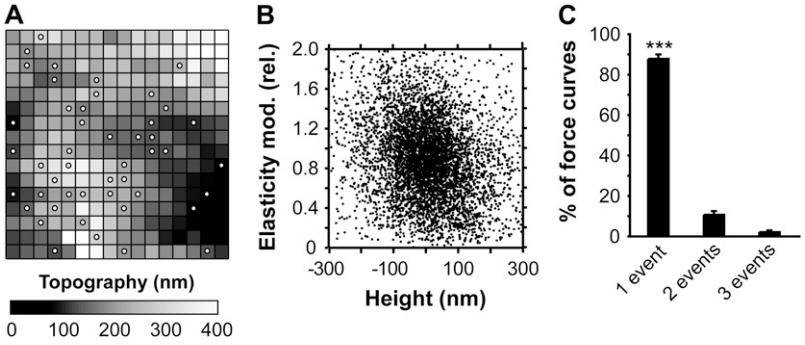

FIGURE 3 Topography, elasticity, and receptor mapping on nonstimulated neurons. (*A*) Topographic map of a scanned cell surface (2×2 μm; one subdivision is 125×125 nm). White circles mark detected binding-unbinding event between the anti-HA tip and HA-tagged AMPARs. The area was scanned line by line, from bottom left to top right. (*B*) Local relative elasticity modulus of the cell as a function of the topographical height. For each cells ($n = 30$), the mean height was put as the 0-nm reference and the mean elasticity was settle to 1. Elasticity and topography distributions showed no correlations. (*C*) Relative percentage of force curves that displayed one, two, or three binding-unbinding events. Single events were the predominant cases, *** $P < 0.0001$, *t*-test.

surface with variations of up to 500 nm in the *z* axis. It can be noticed from Fig. 3 *C* that the surface topography did not show particular correlations with the elasticity modulus.

We detected on average 56 ± 3 binding-unbinding events per 4 μm^2 on the soma of GFP/HA-GluR2-cotransfected neurons ($n = 30$ cells). This is $\sim 5\times$ more than has previously been calculated for endogenous extrasynaptic AMPAR using electrophysiological techniques (47), a difference possibly due to the overexpression of HA-GluR2 in our experiments.

Among the retraction force curves displaying binding-unbinding events, 88% showed a single event, reflecting the detection of individual receptor molecules at the surface of neurons; 10% and 2% presented 2 and 3 events, respectively (Fig. 3 *C*). These extremely rare multiple binding-unbinding events ($P < 0.0001$) could reflect the presence of more than one receptor in the area covered by the tip.

Specificity and stability of receptor detection

To verify the specificity of HA-tagged AMPAR detection, we scanned GFP/HA-GluR2-cotransfected neurons with tips coated with anti-myc antibodies instead of anti-HA. On average, only 2 ± 1 ($n = 10$ cells) binding-unbinding events were recorded with anti-myc coated tips (Fig. 4 *A*), which was significantly lower than the number of events detected with anti-HA tips (56 ± 3, $n = 30$ cells, *t*-test $P < 0.0001$). In a second set of control experiments, tips coated with anti-HA antibodies were used to scan neurons transfected with GFP only instead of GFP and HA-GluR2. GFP transfected cells ($n = 19$ cells) yielded only 4 ± 2 binding-unbinding events (Fig. 4 *A*). This value was statistically highly different from the number of events recorded on GFP/HA-GluR2-cotransfected neurons with anti-HA tips (56 ± 3, $n = 30$ cells, *t*-test $P < 0.0001$). Therefore, we concluded from these experiments that the events detected on GFP/HA-GluR2-cotransfected neurons with anti-HA tips resulted from specific binding-unbinding events between antibodies on the tip and HA-tagged AMPARs at the cell surface.

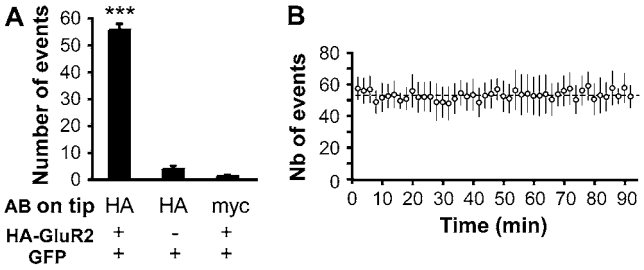

FIGURE 4 Specificity and stability of receptor detection. (*A*) Mean number of binding-unbinding events detected on neurons transfected with GFP and HA-GluR2 or with GFP alone, and scanned with AFM tips coated with HA or myc antibodies (*AB on tip*), as indicated. Error bars are mean ± SE; *n*-values are 30, 19, and 10 cells from left to right. (*B*) Number of binding-unbinding events detected on repeated scans on GFP/HA-GluR2-cotransfected cells ($n = 6$) during 90 min (duration of one scan was 2 min). The number remained constant at 51 ± 2 (*dashed line*).

To demonstrate the stability of functionalized anti-HA tips, we performed, in a different experiment, serial recordings during 90 min over the same area (46 consecutive scans) at the surface of GFP/HA-GluR2-cotransfected neurons. These measurements resulted in a stable number of binding-unbinding events along time, with a mean value of 51 ± 2 events ($n = 6$ cells, Fig. 4 *B*). Moreover, optical inspections with an inverted microscope showed that the cell morphology was not affected by these repetitive scans. These results demonstrated, therefore, that the tip functionality was not altered and that the average number of HA-tagged AMPARs at the surface remained constant during that time range.

AMPARs are located in stiff nanodomains

To investigate whether receptor presence at the cell surface would coincide with particular biophysical properties of the cell, we then analyzed the relative elasticity moduli measured at the tip-receptor binding sites (receptor sites), at its close vicinity (vicinity sites, at 250 nm), and at surface sites distant from receptor (distant sites, farther than 250 nm). The resulting elasticity profile at steady state (Fig. 5 *A*) showed that receptor sites had on average an elasticity modulus $24 \pm 2\%$ higher relative to their vicinity sites ($P < 0.0001$, *t*-test). This value was stable during a 90-min recording (Fig. 5 *B*). Interestingly, vicinity sites had a mean elasticity modulus slightly, but significantly, lower than distant sites ($P < 0.05$, *t*-test). These results suggested, therefore, that AMPARs were

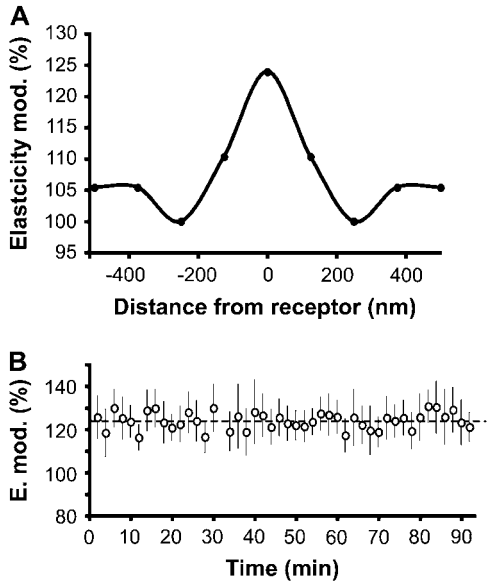

FIGURE 5 AMPARs at steady state are inserted in a nanoenvironment of high relative elasticity modulus. (*A*) Averaged elasticity profile at and around receptor sites. The value measured for vicinity site (at 250 nm) was taken as the 100 reference for elasticity modulus. The profile was smoothened and symmetrically extrapolated. (*B*) Relative elasticity moduli of AMPAR sites were on average 24 ± 2% higher relative to the vicinity sites at 250 nm. Dashed line is the average value for $n = 6$ cells, measured during 90 min. Error bars are mean ± SE.

inserted in stiff nanoenvironments of higher elasticity modulus, surrounded by an immediate vicinity of slightly lower elasticity modulus, compared to the whole surface.

Stimulation-induced trafficking of AMPARs

To study the trafficking of AMPARs, we scanned transfected neurons that were briefly stimulated with NMDA ($n = 5$ cells), which is known to induce AMPAR internalization (3). As a control experiment, we stimulated the cells with vehicle alone ($n = 6$ cells). During 30 min preceding the NMDA stimulation, the number of binding-unbinding events was stable with an average of 51 ± 2 events (Fig. 6 *A*). On cells receiving only the vehicle solution, the number of binding-unbinding events remained constant during the following 60 min (Fig. 6 *A*, *solid triangles*). In contrast, NMDA stimulation provoked a dramatic decrease of the number of binding-unbinding events within 10 min following the stimulation (Fig. 6 *A*, *open circles*). The number of events remained low, with an average value of 24 ± 2, which was significantly lower than the control situation (52 ± 2, $P < 0.0001$; measured between 10 and 60 min after the stimulation). Thus, ~53% of the AMPAR were internalized following NMDA stimulation, without reappearance at the cell surface. These results provide a direct count of the number of individual single receptors being internalized following NMDA stimulation, and are in agreement with previous image analysis data based on confocal microscopy studies (3,8).

It has previously been reported that NMDA stimulation, in the presence of TTX (a Na^{2+} channel blocker that prevents spontaneous neuronal activity) induces AMPAR internalization and subsequent recycling to the membrane (5,8,37). Therefore, we tested the effect of TTX incubation (2 μM, 60 min), before NMDA stimulation, on the detection of receptors. During preincubation with TTX, a stable level of 50 ± 2 binding-unbinding events was detected (Fig. 6 *B*). Application of NMDA (Fig. 6 *B*, *open circle*) provoked again a significant reduction of the number of binding-unbinding events (33 ± 5 at 8 min) compared to vehicle control (49 ± 6 events, $P < 0.03$), with the lowest level at 16 min poststimulation (21 ± 3, $P < 0.001$). In contrast to treatment with NMDA alone, with TTX/NMDA the number of events increased again at later time points and reached control values after 30 min

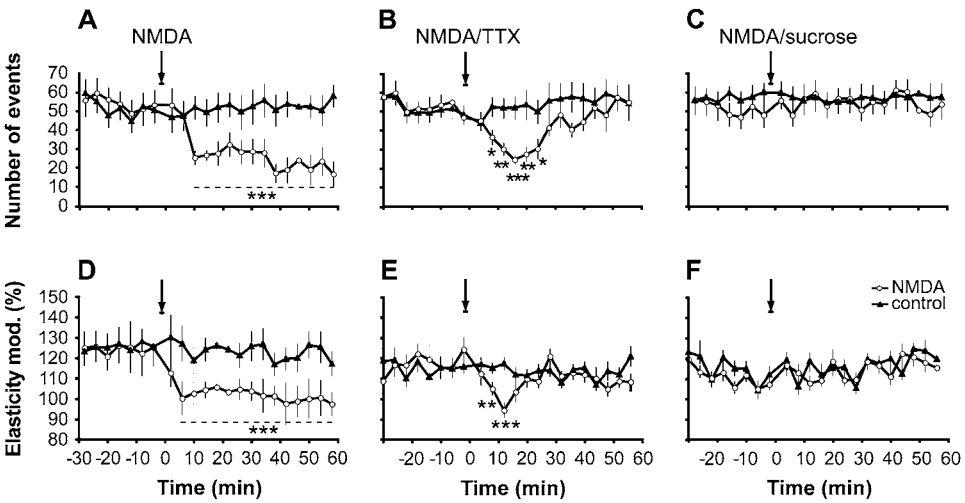

FIGURE 6 On-line trafficking of AMPAR and elasticity measurements at the surface of living hippocampal neurons. (*A*) Number of detected binding-unbinding events (representing AMPARs) at the surface of GFP/HA-GluR2-cotransfected cells. Cells were stimulated for 2 min (*arrow*) with 50 μM NMDA (*circles*, $n = 5$ cells), or with vehicle alone (control, *triangles*, $n = 6$ cells). (*B*) As in panel *A* except that neurons were preincubated with TTX (2 μM) during 60 min, before stimulation for 2 min with 50 μM NMDA (*circles*, $n = 6$ cells), or with vehicle alone (control, *triangles*, $n = 6$ cells). (*C*) As in panel *A* except that cells were incubated in sucrose buffer (450 mM) to block endocytosis, and then stimulated with 50 μM NMDA (*circles*, $n = 7$ cells) or with vehicle alone (control, *triangles*, $n = 5$ cells). (*D–F*) Elasticity modulus of AMPAR sites relative to their vicinity sites at 250 nm for the experiments described in *A–C*, respectively. Error bars are mean ±SE, * $P < 0.05$, ** $P < 0.01$, *** $P < 0.001$, *t*-test.

(27 ± 6 events at 24 min; 45 ± 7 events at 30 min). These results are in good agreement with the recycling time course of endogenous GluR2 recently described for this stimulation protocol (5,8,37).

To confirm that the decrease of detected surface AMPARs was due to endocytosis, we repeated the experiment in the presence of 0.45 M sucrose, which blocks clathrin-dependent endocytosis (39,48). In this case, NMDA stimulation did not induce any significant decrease in the number of receptors detected at the cell surface (Fig. 6 *C*).

Receptor trafficking and surface elasticity correlations

To determine whether the trafficking behavior of single receptors would correlate with the relative elasticity value at their insertion site, we then analyzed the data for the elasticity of the cell surface. We first verified whether the global cell elasticity, independent of receptor presence, was altered by the applied stimulus. Compared to nonstimulated cells (average elasticity modulus of the scanned areas arbitrarily set to 1), we did not detect any changes, neither with NMDA (0.95 ± 0.12, $n = 5$ cells), nor with TTX/NMDA (0.97 ± 0.10, $n = 6$ cells), nor with sucrose/NMDA (0.98 ± 0.12, $n = 7$ cells) (supplemental Fig. 1, Supplementary Material). This result indicates that the stimuli had no effect on the average global surface stiffness. Upon analysis of local effects on relative elasticity, we found as above that, before stimulation, receptor sites had on average a higher elasticity modulus compared to their vicinity sites (Fig. 6, *D–F*). This finding reflected that receptors were located in a stiff nanoenvironment. Upon stimulation with NMDA (with or without TTX), we recorded an initial softening of the cell surface at the receptor sites compared to vicinity sites (Fig. 6, *D* and *E*), which preceded internalization by ~4 min (compare Fig. 6 *A* with 6 *D*, and Fig. 6 *B* with 6 *E*). The high elasticity nanoenvironment was permanently lost following stimulation with NMDA (Fig. 6 *D*), whereas it was reestablished in cases where TTX was applied before NMDA (Fig. 6 *E*). The timing of this effect clearly corresponds to the kinetics of receptor reinsertion at the membrane. In presence of the endocytosis-inhibitor sucrose, NMDA stimulation did not alter the elasticity of receptor sites (Fig. 6 *F*).

DISCUSSION

In this work, we have used the AFM technology to detect single receptors at the cell surface and to follow their trafficking with or without reinsertion. Transfected living neurons expressing HA-tagged AMPARs at their surface have been probed with an AFM tip functionalized with anti-HA antibodies. We conclude that the binding-unbinding events measured here (see Fig. 2) represent specific interactions between HA-tagged AMPARs and anti-HA tip based on the following reasons. 1), No events are measured when the antibody on the tip is replaced by another unrelated antibody. 2), No events are measured when the cells are transfected with GFP alone (without HA-GluR2). 3), The binding-unbinding events cannot represent a rupture of the covalent bond linking the antibody to the tip since covalent bonds are much stronger than the forces recorded here (49). In addition, if antibodies were pulled out from the tip, the tip would gradually lose its detection ability, which is not the case here. 4), This last consideration also suggests that the force necessary to extract a receptor from its membrane is stronger than the unbinding force; otherwise extracted receptor molecules would cover the tip and diminish its functionality (26).

In this study, we used a pharamacological stimulation to change the distribution of AMPAR present at the cell surface. Indeed, in the presence of NMDA, we observe a clear decrease in the number of surface AMPARs. We attribute this phenomenon to receptor internalization because an endocytic blocker totally prevents the diminution of surface AMPAR number after NMDA stimulation. NMDA does not directly target AMPARs, but another type of glutamate receptors (NMDA receptors). Therefore, NMDA-induced trafficking of AMPAR results from NMDA receptor activation and from subsequent intracellular mechanisms that remain unclear. Interestingly, AMPAR trafficking pathways clearly appear to depend on the level of neuronal endogenous activity. In the presence of TTX, which blocks endogenous activity, receptors are recycled at the membrane within 30 min following NMDA stimulation, whereas in the absence of TTX, no reinsertion is observed. Previously, it has been suggested that NMDA stimulation in the absence of TTX induces AMPAR sorting through the degradation pathway (3,8). This might explain why we did not observe reappearance of the AMPARs at the cell surface after NMDA stimulation alone.

Simultaneous receptor detection and measurements of relative elastic properties show that AMPARs are located in nanodomains stiffer than the surrounding cell surface. It is likely that the differences in nanomechanical properties of the neuronal surface reflect differences in the molecular lipid or protein environments in or at the membrane (50), or characteristics of the underlying cytoskeleton (33,34,51). Interestingly, it has been shown that a subpopulation of AMPARs is localized to particular dynamic domains enriched in cholesterol and sphingolipids, called lipid raft. Lipid rafts are involved in localized signaling at the membrane, trafficking of membranes proteins, and regulation of cortical actin (12,52). It was shown that depletion of cholesterol/sphingolipid leads to instability of surface AMPARs and their removal from the surface. These results are in good agreement with the idea that microdomains such as lipid raft might be involved in the control of AMPAR distribution.

Interestingly, the AMPAR stiff nanodomains are influenced by the NMDA/TTX stimulation that provokes AMPAR internalization and recycling (8). Indeed, the nanodomains disappear a few minutes before receptor endocytosis (on

average 4 min earlier) and are recovered slightly before receptor recycling. However, when recycling does not occur (NMDA alone), AMPARs that remain at the surface are no more contained in stiff nanodomains (Fig. 6 *A*). This suggests that AMPARs that are not internalized might be in a different state compared to unstimulated or recycled receptors. Neural activity could therefore selectively activate AMPARs linked to molecular microenvironments with specific biophysical properties. Although the molecular basis for this mechanism remains to be elucidated, our study revealed the existence of a link between mechanical properties of the cell and differential protein dynamics.

Our results clearly demonstrate that AFM is able to follow receptor distribution on living cells at the level of single molecules. In contrast, the approaches routinely used to study receptor trafficking, such as confocal image analysis (3,8,39) or biotinylation (5), cannot reach the single molecule resolution. Indeed, confocal microscopy studies measure a signal emitted from a large and unknown number of receptors (3,8,39). Similarly biotinylation is based on the quantification of immunoblot, which does not give any access to single molecule quantification (5). In addition, in most of the cases these methods do not allow real-time measurements. Other techniques allow on-line measurements but cannot follow a quantified pool of receptors during a timescale relevant for stimulation-induced trafficking (6,46). Tracking of single fluorescent molecules at the surface of living cells has so far been limited to a few seconds measurements only (53,54). The technology that we present presented here can be extended to any cell type and any receptor presenting an extracellular domain. Therefore, it offers tremendous opportunities to investigate simultaneously biophysical properties of the cell and the dynamics of receptor trafficking at the nanometer scale.

SUPPLEMENTARY MATERIAL

An online supplement to this article is available by visiting BJ Online at http://www.biophysj.org.

We acknowledge Liliane Glauser for excellent technical assistance and J.-C. F. Sarria for help with confocal microscope handling. We thank Hilal Lashuel and Andrzej Kulik for critical reading of the manuscript.

H.H. is supported by grants from the Swiss National Science Foundation (No. 3100AO-100834/1) and from the Leenaards Foundation (No. 1907/ep).

REFERENCES

1. Stevens, C. F., and J. Sullivan. 1998. Synaptic plasticity. *Curr. Biol.* 8:R151–R153.
2. Collingridge, G. L., J. T. Isaac, and Y. T. Wang. 2004. Receptor trafficking and synaptic plasticity. *Nat. Rev. Neurosci.* 5:952–962.
3. Lee, S. H., A. Simonetta, and M. Sheng. 2004. Subunit rules governing the sorting of internalized AMPA receptors in hippocampal neurons. *Neuron.* 43:221–236.
4. Passafaro, M., V. Piech, and M. Sheng. 2001. Subunit-specific temporal and spatial patterns of AMPA receptor exocytosis in hippocampal neurons. *Nat. Neurosci.* 4:917–926.
5. Ehlers, M. D. 2000. Reinsertion or degradation of AMPA receptors determined by activity-dependent endocytic sorting. *Neuron.* 28:511–525.
6. Triller, A., and D. Choquet. 2005. Surface trafficking of receptors between synaptic and extrasynaptic membranes: and yet they do move! *Trends Neurosci.* 28:133–139.
7. Adesnik, H., R. A. Nicoll, and P. M. England. 2005. Photoinactivation of native AMPA receptors reveals their real-time trafficking. *Neuron.* 48:977–985.
8. Steiner, P., S. Alberi, K. Kulangara, A. Yersin, J. C. Sarria, E. Regulier, S. Kasas, G. Dietler, D. Muller, S. Catsicas, and H. Hirling. 2005. Interactions between NEEP21, GRIP1 and GluR2 regulate sorting and recycling of the glutamate receptor subunit GluR2. *EMBO J.* 24:2873–2884.
9. Malinow, R., and R. C. Malenka. 2002. AMPA receptor trafficking and synaptic plasticity. *Annu. Rev. Neurosci.* 25:103–126.
10. Bredt, D. S., and R. A. Nicoll. 2003. AMPA receptor trafficking at excitatory synapses. *Neuron.* 40:361–379.
11. Song, I., and R. L. Huganir. 2002. Regulation of AMPA receptors during synaptic plasticity. *Trends Neurosci.* 25:578–588.
12. Hering, H., C. C. Lin, and M. Sheng. 2003. Lipid rafts in the maintenance of synapses, dendritic spines, and surface AMPA receptor stability. *J. Neurosci.* 23:3262–3271.
13. Binnig, G., C. F. Quate, and C. Gerber. 1986. Atomic force microscope. *Phys. Rev. Lett.* 56:930–933.
14. Engel, A., and D. J. Muller. 2000. Observing single biomolecules at work with the atomic force microscope. *Nat. Struct. Biol.* 7:715–718.
15. Willemsen, O. H., M. M. Snel, A. Cambi, J. Greve, B. G. De Grooth, and C. G. Figdor. 2000. Biomolecular interactions measured by atomic force microscopy. *Biophys. J.* 79:3267–3281.
16. Hinterdorfer, P., and Y. F. Dufrene. 2006. Detection and localization of single molecular recognition events using atomic force microscopy. *Nat. Methods.* 3:347–355.
17. Fisher, T. E., A. F. Oberhauser, M. Carrion-Vazquez, P. E. Marszalek, and J. M. Fernandez. 1999. The study of protein mechanics with the atomic force microscope. *Trends Biochem. Sci.* 24:379–384.
18. Samori, B., G. Zuccheri, and R. Baschieri. 2005. Protein unfolding and refolding under force: methodologies for nanomechanics. *ChemPhysChem.* 6:29–34.
19. Radmacher, M. 2002. Atomic force microscopy in cell biology. *In* Methods in Cell Biology. B. P. Jena, and J. K. H. Hörber, editors. Academy Press, San Diego, CA. 67–90.
20. Yersin, A., H. Hirling, P. Steiner, S. Magnin, R. Regazzi, B. Huni, P. Huguenot, P. De los Rios, G. Dietler, S. Catsicas, and S. Kasas. 2003. Interactions between synaptic vesicle fusion proteins explored by atomic force microscopy. *Proc. Natl. Acad. Sci. USA.* 100:8736–8741.
21. Bonanni, B., A. S. Kamruzzahan, A. R. Bizzarri, C. Rankl, H. J. Gruber, P. Hinterdorfer, and S. Cannistraro. 2005. Single molecule recognition between cytochrome C 551 and gold-immobilized azurin by force spectroscopy. *Biophys. J.* 89:2783–2791.
22. Schwesinger, F., R. Ros, T. Strunz, D. Anselmetti, H. J. Guntherodt, A. Honegger, L. Jermutus, L. Tiefenauer, and A. Pluckthun. 2000. Unbinding forces of single antibody-antigen complexes correlate with their thermal dissociation rates. *Proc. Natl. Acad. Sci. USA.* 97:9972–9977.
23. Bustanji, Y., C. R. Arciola, M. Conti, E. Mandello, L. Montanaro, and B. Samori. 2003. Dynamics of the interaction between a fibronectin molecule and a living bacterium under mechanical force. *Proc. Natl. Acad. Sci. USA.* 100:13292–13297.
24. Pfister, G., C. M. Stroh, H. Perschinka, M. Kind, M. Knoflach, P. Hinterdorfer, and G. Wick. 2005. Detection of HSP60 on the membrane surface of stressed human endothelial cells by atomic force and confocal microscopy. *J. Cell Sci.* 118:1587–1594.
25. Trache, A., J. P. Trzeciakowski, L. Gardiner, Z. Sun, M. Muthuchamy, M. Guo, S. Y. Yuan, and G. A. Meininger. 2005. Histamine effects on

endothelial cell fibronectin interaction studied by atomic force microscopy. *Biophys. J.* 89:2888–2898.

26. Ikai, A. 2004. Nanomechanics of protein-based biostructures. *Jpn. J. Appl. Phys. 1.* 43:7365–7375.
27. Afrin, R., T. Yamada, and A. Ikai. 2004. Analysis of force curves obtained on the live cell membrane using chemically modified AFM probes. *Ultramicroscopy.* 100:187–195.
28. Oesterhelt, F., D. Oesterhelt, M. Pfeiffer, A. Engel, H. E. Gaub, and D. J. Muller. 2000. Unfolding pathways of individual bacteriorhodopsins. *Science.* 288:143–146.
29. Lehenkari, P. P., G. T. Charras, A. Nykanen, and M. A. Horton. 2000. Adapting atomic force microscopy for cell biology. *Ultramicroscopy.* 82:289–295.
30. Osada, T., A. Itoh, and A. Ikai. 2003. Mapping of the receptor-associated protein (RAP) binding proteins on living fibroblast cells using an atomic force microscope. *Ultramicroscopy.* 97:353–357.
31. Almqvist, N., R. Bhatia, G. Primbs, N. Desai, S. Banerjee, and R. Lal. 2004. Elasticity and adhesion force mapping reveals real-time clustering of growth factor receptors and associated changes in local cellular rheological properties. *Biophys. J.* 86:1753–1762.
32. Radmacher, M., M. Fritz, C. M. Kacher, J. P. Cleveland, and P. K. Hansma. 1996. Measuring the viscoelastic properties of human platelets with the atomic force microscope. *Biophys. J.* 70:556–567.
33. Kasas, S., X. Wang, H. Hirling, R. Marsault, B. Huni, A. Yersin, R. Regazzi, G. Grenningloh, B. Riederer, L. Forro, G. Dietler, and S. Catsicas. 2005. Superficial and deep changes of cellular mechanical properties following cytoskeleton disassembly. *Cell Motil. Cytoskeleton.* 62:124–132.
34. Rotsch, C., and M. Radmacher. 2000. Drug-induced changes of cytoskeletal structure and mechanics in fibroblasts: an atomic force microscopy study. *Biophys. J.* 78:520–535.
35. A-Hassan, E., W. F. Heinz, M. D. Antonik, N. P. D'Costa, S. Nageswaran, C. A. Schoenenberger, and J. H. Hoh. 1998. Relative microelastic mapping of living cells by atomic force microscopy. *Biophys. J.* 74:1564–1578.
36. Schrot, S., C. Weidenfeller, T. E. Schaffer, H. Robenek, and H. J. Galla. 2005. Influence of hydrocortisone on the mechanical properties of the cerebral endothelium in vitro. *Biophys. J.* 89:3904–3910.
37. Steiner, P., J. C. Sarria, L. Glauser, S. Magnin, S. Catsicas, and H. Hirling. 2002. Modulation of receptor cycling by neuron-enriched endosomal protein of 21 kD. *J. Cell Biol.* 157:1197–1209.
38. Xia, Z., H. Dudek, C. K. Miranti, and M. E. Greenberg. 1996. Calcium influx via the NMDA receptor induces immediate early gene transcription by a MAP kinase/ERK-dependent mechanism. *J. Neurosci.* 16:5425–5436.
39. Carroll, R. C., E. C. Beattie, H. Xia, C. Luscher, Y. Altschuler, R. A. Nicoll, R. C. Malenka, and M. von Zastrow. 1999. Dynamin-dependent endocytosis of ionotropic glutamate receptors. *Proc. Natl. Acad. Sci. USA.* 96:14112–14117.
40. Hirling, H., P. Steiner, C. Chaperon, R. Marsault, R. Regazzi, and S. Catsicas. 2000. Syntaxin 13 is a developmentally regulated SNARE involved in neurite outgrowth and endosomal trafficking. *Eur. J. Neurosci.* 12:1913–1923.
41. Hutter, J. L., and J. Bechhoefer. 1993. Calibration of atomic-force microscope tips. *Rev. Sci. Instrum.* 64:1868–1873.
42. Chtcheglova, L. A., G. T. Shubeita, S. K. Sekatskii, and G. Dietler. 2004. Force spectroscopy with a small dithering of AFM tip: a method of direct and continuous measurement of the spring constant of single molecules and molecular complexes. *Biophys. J.* 86:1177–1184.
43. Laurent, V. M., S. Kasas, A. Yersin, T. E. Schaffer, S. Catsicas, G. Dietler, A. B. Verkhovsky, and J. J. Meister. 2005. Gradient of rigidity in the lamellipodia of migrating cells revealed by atomic force microscopy. *Biophys. J.* 89:667–675.
44. Kasas, S., B. M. Riederer, S. Catsicas, B. Cappella, and G. Dietler. 2000. Fuzzy logic algorithm to extract specific interaction forces from atomic force microscopy data. *Rev. Sci. Instrum.* 71:2082–2086.
45. Heinz, W. F., and J. H. Hoh. 1999. Spatially resolved force spectroscopy of biological surfaces using the atomic force microscope. *Trends Biotechnol.* 17:143–150.
46. Shi, S., Y. Hayashi, J. A. Esteban, and R. Malinow. 2001. Subunit-specific rules governing AMPA receptor trafficking to synapses in hippocampal pyramidal neurons. *Cell.* 105:331–343.
47. Cottrell, J. R., G. R. Dube, C. Egles, and G. Liu. 2000. Distribution, density, and clustering of functional glutamate receptors before and after synaptogenesis in hippocampal neurons. *J. Neurophysiol.* 84: 1573–1587.
48. Heuser, J. E., and R. G. Anderson. 1989. Hypertonic media inhibit receptor-mediated endocytosis by blocking clathrin-coated pit formation. *J. Cell Biol.* 108:389–400.
49. Grandbois, M., M. Beyer, M. Rief, H. Clausen-Schaumann, and H. E. Gaub. 1999. How strong is a covalent bond? *Science.* 283:1727–1730.
50. Frankel, D. J., J. R. Pfeiffer, Z. Surviladze, A. E. Johnson, J. M. Oliver, B. S. Wilson, and A. R. Burns. 2006. Revealing the topography of cellular membrane domains by combined AFM/fluorescence imaging. *Biophys. J.* 90:2404–2413.
51. Wu, H. W., T. Kuhn, and V. T. Moy. 1998. Mechanical properties of L929 cells measured by atomic force microscopy: effects of anti-cytoskeletal drugs and membrane crosslinking. *Scanning.* 20:389–397.
52. Simons, K., and D. Toomre. 2000. Lipid rafts and signal transduction. *Nat. Rev. Mol. Cell Biol.* 1:31–39.
53. Tardin, C., L. Cognet, C. Bats, B. Lounis, and D. Choquet. 2003. Direct imaging of lateral movements of AMPA receptors inside synapses. *EMBO J.* 22:4656–4665.
54. Groc, L., M. Heine, L. Cognet, K. Brickley, F. A. Stephenson, B. Lounis, and D. Choquet. 2004. Differential activity-dependent regulation of the lateral mobilities of AMPA and NMDA receptors. *Nat. Neurosci.* 7:695–696.